Tissue Eng Regen Med (2022) 19(2):289–299
https://doi.org/10.1007/s13770-021-00385-6

Online ISSN 2212-5469

ORIGINAL ARTICLE

Metal Ion Releasing Gold Nanoparticles for Improving Therapeutic Efficiency of Tumor Targeted Photothermal Therapy

Jung Hwan Park[1] · Euiyoung Jung[2] · Hyeonji Lim[2] · Ju-Ro Lee[3] · Yoon Ki Joung[3,4] · Taekyung Yu[2] · Suk Ho Bhang[1]

Received: 16 July 2021 / Revised: 5 August 2021 / Accepted: 8 August 2021 / Published online: 24 September 2021

Abstract

BACKGROUND: Owing to the tumor-targeted migration capacity of human mesenchymal stem cells (hMSCs), they have been combined with nanoparticles for photothermal therapy. However, the low viability of hMSCs following transplantation remains a problem. Here, we developed iron (Fe) ion-releasing gold (Au) nanoparticles (IIAuNPs) for advanced tumor-targeted photothermal therapy using hMSCs.

METHODS: IIAuNPs were designed to undergo degradation under low pH conditions, such as the endosomal microenvironment, for Fe ion release in hMSCs. After evaluating the properties of IIAuNP, the IIAuNP concentration for treating hMSCs was optimized in terms of cytotoxicity. *In vitro* cell migration and antiapoptotic factor secretion were observed in hMSCs. Additionally, IIAuNPs-treated hMSCs were intravenously injected into tumor-bearing mice, and enhanced tumor targeting based on improved cell viability and cell migration was evaluated. Three days after the injection, the mice were irradiated with 660 nm laser to confirm the enhanced photothermal effect.

RESULTS: *In vitro* studies revealed that treating hMSCs with an optimum concentration of IIAuNPs enhanced cell migration and anti-apoptotic gene expression through intracellular Fe ion delivery. The viability of hMSCs under hypoxic cell culture conditions that mimic the *in vivo* microenvironment was also improved when hMSCs were treated with IIAuNPs, compared to hMSCs without IIAuNPs treatment. IIAuNPs-treated hMSCs showed significantly enhanced tumor-targeting efficiency and subsequent photothermal effect compared to hMSCs without IIAuNP treatment.

CONCLUSION: Our results suggest that our metal-ion-releasing photothermal nanoparticles may provide a promising platform for future photothermal therapies and related applications.

Keywords Human mesenchymal stem cell · Metal ion delivery · Photothermal therapy

Jung Hwan Park and Euiyoung Jung have contributed equally to this work.

✉ Taekyung Yu
tkyu@khu.ac.kr

✉ Suk Ho Bhang
sukhobhang@skku.edu

[1] School of Chemical Engineering, Sungkyunkwan University, 2066, Seobu-ro, Jangan-gu, Suwon 16419, Republic of Korea

[2] Department of Chemical Engineering, College of Engineering, Integrated Engineering Major, Kyung Hee University, 1732 Deogyeong-daero, Giheung-gu, Yongin 17140, Republic of Korea

[3] Center for Biomaterials, Biomedical Research Institute, Korea Institute of Science and Technology, Hwarang-ro 14-gil 5, Seoungbuk-gu, Seoul 02792, Republic of Korea

[4] Division of Bio-Medical Science & Technology, University of Science and Technology, 113 Gwahangno, Yuseong-gu, Daejeon 305-333, Republic of Korea

1 Introduction

Photothermal therapy (PTT) generates heat because of irradiating light to selectively remove abnormal cells or tissues. In contrast to chemotherapy and conventional radiation therapy, PTT can minimize the side effects on normal cells by targeting tumor cells [1]. When high-power or low-power lasers are used, heat by irradiation induces unwanted tissue damage or does not kill tumor cells, respectively [2–4]. Therefore, laser irradiation with appropriate power is required for PTT. Recently, gold nanoparticles (AuNPs) have garnered attention as reagents for PTT [5–7]. AuNPs have the ability to convert light energy into heat by localized surface plasmon resonance (LSPR). When the surface of AuNPs is irradiated with light, a collective vibration of electrons occurs due to the interaction of light and electrons at a specific wavelength, and heat is generated. AuNPs can easily manipulate the LSPR wavelength by controlling their structure, shape, and size [8]. Near-infrared (NIR) light is the most common light source for PTT because NIR can transmit deeper into the body on account of its low absorbance by molecules in the body [9]. AuNPs have several advantages as a reagent for PTT, as they interact with NIR and are inert in the body.

However, insufficient heat that cannot destroy the tumor often remains a critical limitation because of the low tumor-targeting efficiency of unmodified AuNPs. To address this problem, human mesenchymal stem cells (hMSCs) have been studied as carriers of AuNPs [5]. hMSCs are known to move toward injury and tumor sites by chemotaxis [5, 10, 11]. As a large number of chemokines are secreted from tumors, circulating hMSCs can recognize and move toward the tumor tissues. In particular, C-X-C chemokine receptor type 4 (CXCR4) in hMSCs greatly contributes to their migration to the tumor site by binding to chemokines. hMSCs that recognize chemokines move along the inner wall of blood vessels and penetrate tumor tissues. Therefore, upregulation of CXCR4 expression in hMSCs might be a key factor for improving tumor targeting efficiency [10–12]. Additionally, low cell viability after intravenous injection of hMSCs can decrease tumor targeting efficiency. Therefore, a novel method that can improve both the tumor targeting efficiency and cell viability of hMSCs is required.

Here, we fabricated iron (Fe) ion-releasing AuNPs (IIAuNPs) to augment the tumor-targeting efficiency and cell viability of hMSCs for advanced PTT (Fig. 1). Fe, a transition metal, has lower reduction potential than Au. Therefore, when IIAuNPs are incorporated into hMSCs through endocytosis, they release Fe ions due to its lower reduction potential than that of Au and low pH conditions in endosomes (pH 4–5) [13, 14]. Fe ions from released from IIAuNPs promote the expression of CXCR4, vascular endothelial growth factor (VEGF), and basic fibroblast growth factor (FGF2), which increases the targeting efficiency and prolongs the cell survival rate after intravenous injection of hMSCs [15–18]. In the present study, we fabricated and incorporated IIAuNPs into hMSCs. Treating the hMSCs with the optimized concentration of IIAuNPs (IIAuNPs-hMSCs) successfully generated sufficient heat for PTT without causing cytotoxicity *in vitro*. Additionally, IIAuNPs upregulated the expression of anti-apoptotic growth factors (VEGF and FGF2) and CXCR4 in hMSCs which resulted in an increase in the survival rate and migration ability *in vitro*. Finally, intravenously injected

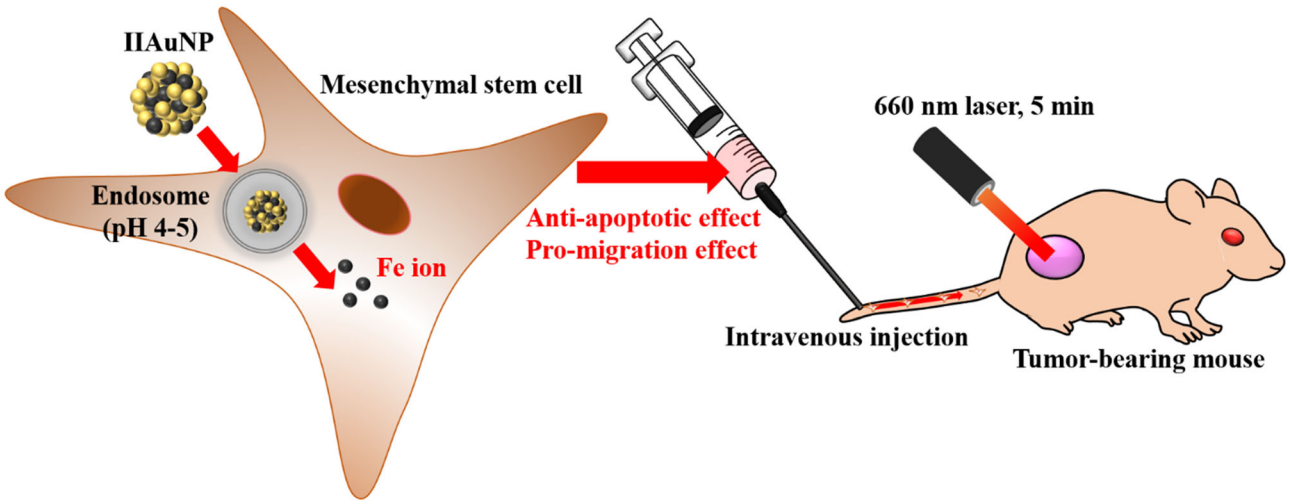

Fig. 1 Schematic of PTT using IIAuNP. Fe is dispersed as ions due to the low endosomal pH. Fe ions enhanced the secretion of anti-apoptotic paracrine factors from hMSCs. Enhanced cell viability and cell migration ability led to improved tumor targeting efficiency of hMSCs and improved therapeutic effect of PTT based on IIAuNPs

IIAuNPs-hMSCs with exogenous laser irradiation significantly decreased the size of the tumor and inhibited further recurrence. Together, our method paves the way for a new approach using metal-ion-releasing photothermal nanoparticles for PTT.

2 Materials and methods

2.1 Cells

hMSCs were purchased from Lonza (Allendale, NJ, USA). The human fibrosarcoma cell line HT-1080 was purchased from American Type Culture Collection (ATCC; Manassas, VA, USA). Both types of cells were cultured in Dulbecco's modified Eagle's medium (Gibco BRL, Grand Island, NY, USA). The cell culture medium was supplemented with 10% (v/v) fetal bovine serum (Gibco BRL) and 1% (v/v) penicillin/streptomycin (Gibco BRL). Both cells were incubated at 37 °C under 5% CO_2. Cell culture medium was replenished every two days. hMSCs within four passages were used in the experiments.

2.2 Synthesis of IIAuNPs

To synthesize IIAuNPs, 1 mL of sodium borohydride ($NaBH_4$, Sigma-Aldrich, St. Louis, MO, USA) solution (4 mg/mL) was added to 9 mL of deionized (DI) water containing 100 mg of poly(vinyl pyrrolidone) (PVP, Sigma-Aldrich) under magnetic stirring with 600 rpm. 4 mg of gold (III) chloride hydrate ($HAuCl_4{\cdot}xH_2O$, Sigma-Aldrich) in 1 mL and 2 mg of iron (III) chloride ($FeCl_3$, Sigma-Aldrich) in 1 mL were slowly co-injected into the reacting solution. After 15 min, the product was collected by centrifugation using acetone (Daejung Chem. & Metals, Siheung, Korea) at 9000 rpm for 15 min. After several washing process, the product was dispersed in DI water. The entire reaction was performed at room temperature. To synthesize AuNPs, the reaction conditions were the same except for the absence of iron (III) chloride solution.

2.3 Characterization of IIAuNPs

Transmission electron microscopy (TEM) was performed, and energy-dispersive X-ray spectroscopy (EDS) spectra were obtained using a JEM-2100F transmission electron microscope (JEOL, Tokyo, Japan) at 200 kV. X-ray diffraction (XRD) patterns were obtained using a D-MAX/A diffractometer (35 kV, 35 mA, Rigaku, Tokyo, Japan). UV–vis spectra were obtained using a Shimadzu 2550 spectrophotometer (Shimadzu, Kyoto, Japan). The atomic ratios of Au and Fe were determined using EDS and a direct reading echelle inductively coupled plasma (ICP) spectrometer (Leeman, Hudson, NH, USA). Various amounts of IIAuNPs were diluted with phosphate buffer saline (PBS) and irradiated using a 660 nm and 808 nm continuous wave (CW) laser beam (UNIOTECH, Daejeon, Korea) with an output power of 2 W/cm^2. The temperature and photothermal images of the IIAuNP suspensions were recorded with an infrared thermal imaging system (30 s periodical evaluation, FLIR E4, FLIR Systems Inc., Wilsonville, OR, USA).

2.4 Cytotoxicity analysis

Cell viability was evaluated using the Cell Counting kit-8 (CCK-8, Dojindo Molecular Technologies, Inc., Kumamoto, Japan). Briefly, hMSCs (1×10^4 cells/well) were cultured in 24-well plates with IIAuNPs for 24 h and rinsed with PBS three times. After changing the wells with fresh medium, CCK-8 solution was added. After 2 h of incubation, the absorbance at 450 nm was measured using an Infinite F50 plate reader (Tecan, Zürich, Switzerland). The cell viability was calculated to be proportional to the results from IIAuNP-untreated cells (n = 4 per group).

2.5 Apoptotic activity and hypoxic culture of the hMSCs

The hMSCs were seeded on 6-well plates (1×10^5 cells/well) for 24 h and various concentrations of IIAuNPs were applied. A live and dead assay kit (Sigma) was used to observe live and dead cells through signals from fluorescein diacetate (FDA) and ethidium bromide (EB)-stained cells, respectively, according to the manufacturer's protocol. Apoptotic index defined as the percentage (%) of apoptotic cells was calculated according to the formula: The number of EB^+ cells × 100/Total number of cells [19]. Terminaldeoxynucleotide transferase-mediated deoxyuridine triphosphate nick end labeling assay (TUNEL assay) was performed on the cultures using TUNEL assay kit (ApopTag® fluorescent in situ apoptosis detection kit, Millipore, Bedford, MA, USA), according to the manufacturer's protocol. FDA/EB and TUNEL assay results were evaluated by fluorescence microscopy (DMi8, Leica, Wetzlar, Germany). To generate hypoxic culture conditions for the growth of hMSCs, culture dishes were placed in a hypoxic incubator (VS-9260GC, Vision, Bucheon, Korea) for 48 h with 1% O_2, 5% CO_2, and 37 °C condition [20].

2.6 Quantitative reverse-transcription polymerase chain reaction (qRT-PCR)

Relative gene expression levels were evaluated by qRT-PCR. Human specific glyceraldehyde-3-phosphate

dehydrogenase (GAPDH), VEGF, FGF2, CXCR4, Caspase-3, and Bcl-XL were used. Total ribonucleic acid (RNA) was collected using TRIzol reagent (1 mL, Life Technologies, Inc., Carlsbad, CA, USA) and chloroform (200 μL). The lysed samples were centrifuged, and the RNA pellets were washed with 35% (v/v) ethanol in water and dried. The samples were then dissolved in RNase-free water. qRT-PCR was then performed using the SsoAdvanced™ Universal SYBR Green Supermix kit (Bio-Rad, Hercules, CA, USA).

2.7 Migration assay

hMSCs were seeded onto 6-well plates. The cells were incubated with or without IIAuNPs for 1 h. Using a P200 pipette tip, a straight scratch was induced on the hMSCs. The cells were washed and cultured in a serum-free medium. After incubation for 0 and 18 h, the repopulated area was measured and compared to the initial empty space at 0 h [21]. The Photoshop CC program (Adobe Systems, San Jose, CA, USA) was used to acquire data as previously described [22].

2.8 *In vitro* photothermal effect and intracellular loading of IIAuNPs

To evaluate the *in vitro* photothermal effects, hMSCs were incubated with IIAuNPs. After rinsing three times with PBS, the hMSCs treated with IIAuNPs (IIAuNPs-hMSCs) were retrieved through trypsin treatment and 660 nm laser irradiation for 5 min. The temperature and photothermal images of the IIAuNPs-hMSCs were recorded using an infrared thermal imaging system (every 1 min). The hMSCs were incubated with IIAuNPs for 1 h, rinsed with PBS three times, and collected via trypsinization. Suspended cells were lysed using aqua regia. The amounts of gold and iron in the lysates were determined using an ICP-OES analyzer (Varian, Mulgrave, Australia). Additionally, the amount of gold in the tumor after intravenous injection of hMSCs with or without IIAuNP treatment and in IIAuNPs alone was evaluated three days after the *in vivo* injection, using the ICP-OES (Varian) with the same method.

2.9 Mouse modeling

Athymic nude mice (6 weeks, BABL/c, female, Orient Bio, Seoul, Korea) were used for *in vivo* experiments. After anesthetizing the mice using a mixture of xylazine (10 mg/kg, Rompun; Bayer Korea, Ansan, Korea) and ketamine hydrochloride (100 mg/kg, ketamine, Yuhan, Seoul, Korea), HT-1080 cells (5×10^6 cells / 100 μL PBS) were subcutaneously injected into both flanks of the mice. Mice bearing tumors with diameters greater than 3.5 mm were selected for further experiments. The animal study was approved by the Institutional Animal Care and Use Committee of SungKyunKwan University (SKKUIACUC 2017–05-03–3).

2.9.1 In vivo photothermal tumor therapy

PBS (100 μL), hMSCs (1×10^6 cells/100 μL PBS), IIAuNPs (44.42 μg Fe/100 μL PBS), or IIAuNPs-hMSC (1×10^6 cells with IIAuNPs/100 μL PBS) were intravenously injected into the tumor-induced mice. Every mouse in the IIAuNP and IIAuNP-hMSC groups received the same amount of IIAuNPs (44.42 μg Fe). Three days after the injection, the tumor tissues were irradiated with a 660 nm laser for 5 min under anesthesia. FLIR E4 was used to record temperature variations in the tumor regions. The tumor volume was calculated using the formula $V = A \times B^2 \times 0.5$, where A and B indicate the largest and smallest diameters, respectively.

2.9.2 Statistical analysis

Statistical analysis was performed with ANOVA and Tukey's significant difference post hoc test using SPSS software (SPSS Inc., USA). Results are expressed as mean ± standard deviation. Statistical significance was set at $p < 0.05$.

3 Result

3.1 Characterization of IIAuNPs

TEM imaging showed that the IIAuNPs had a spherical shape with an average size of 3.06 nm (Fig. 2A, B). The EDS spectrum revealed the co-presence of Fe and Au in the IIAuNPs (Fig. 2C). XRD patterns of the IIAuNPs were slightly shifted to higher angles compared to those of AuNPs due to the different atomic sizes of Au and Fe (Fig. 2D). In addition, red-shift of the plasmon resonance occurred because of the presence of Fe atoms in the UV–vis spectra (Fig. 2E). Both XRD and UV–vis strongly indicated that the nanoparticles contained both Fe and Au. The metal ion dissolution experiment showed that Fe ions were released from IIAuNPs under acidic conditions when IIAuNPs were stored under neutral and acidic conditions for 12 h (Fig. 2F). At Fe concentrations of 5 μg/100 μL and 15 μg/100 μL, the wavelength of the laser at which the photothermal effect occured was confirmed. On irradiation with a 660 nm laser at 5 μg/100 μL, temperature increased to 60.625 °C in 1 min, but only to 51.5 °C when an 808 nm laser was used (Fig. 2G). At 15 μg/100 μL,

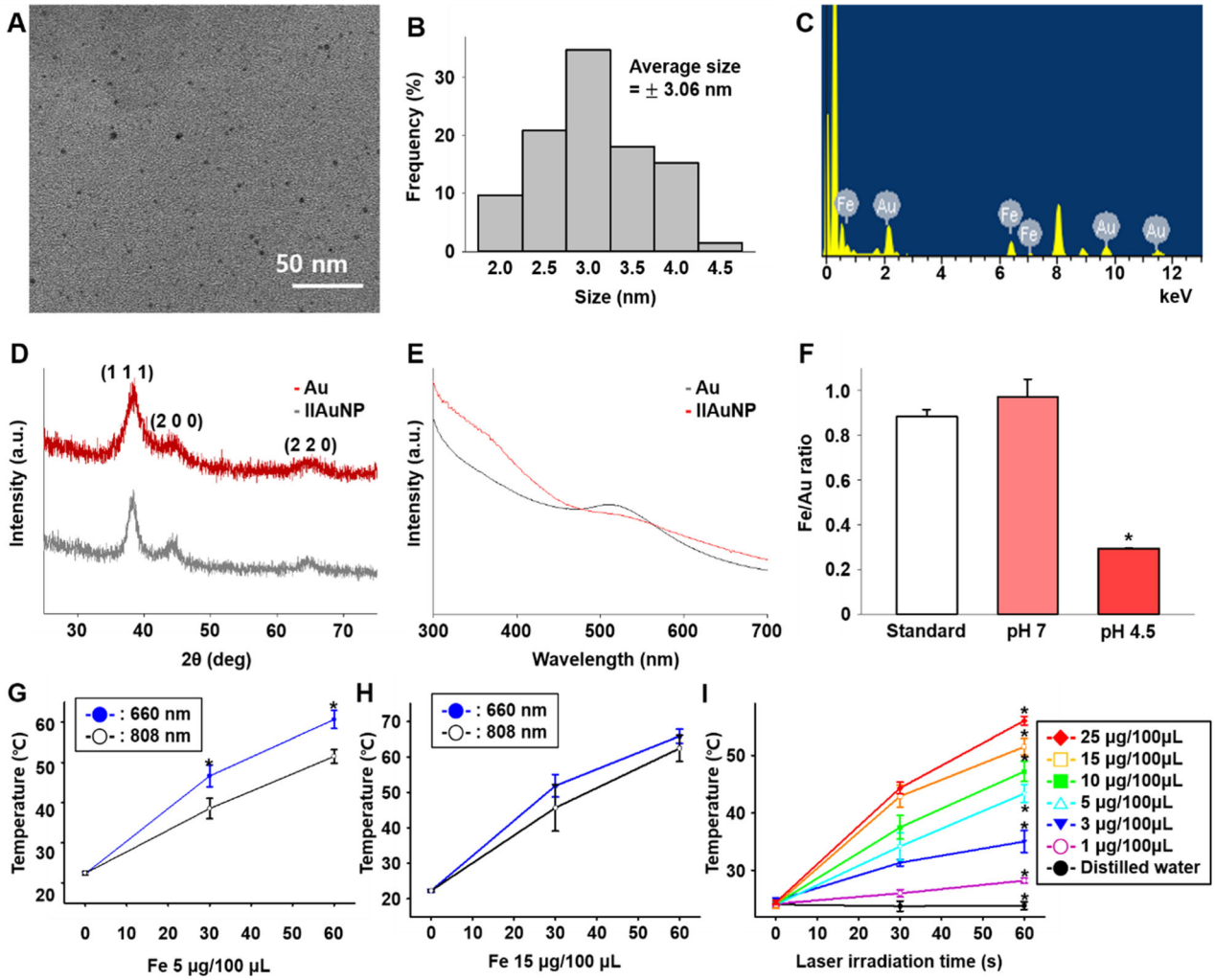

Fig. 2 Characterization of IIAuNP. **A** TEM image of IIAuNPs. **B** Size distribution of IIAuNPs. **C** EDS spectrum of IIAuNPs. **D** XRD patterns of AuNPs (lower line) and IIAuNPs (upper line). **E** UV–vis spectra of AuNPs and IIAuNPs. **F** Atomic ratio change of Fe/Au of IIAuNPs stored at different pH for 12 h, measured using EDS (n = 3, $^*p < 0.001$ versus all other groups). **G, H** Temperature increase due to laser irradiation of specific concentrations of IIAuNPs. **I** Temperature change through 660 nm laser irradiation according to concentration change of IIAuNPs

temperature rose to 65.85 °C in 1 min when irradiated with a 660 nm laser, but only to 62.42 °C with the 808 nm laser (Fig. 2H). On using the 660 nm laser at both concentrations, the temperature increased significantly. On irradiating the 660 nm laser, the temperature increased as the concentration of IIAuNPs increased. There was no change in temperature in distilled water, however, when the Fe concentration of IIAuNPs was 25 μg/100 μL, the temperature increaed to 56 °C over 1 min (Fig. 2I).

3.2 Cytotoxic effects of IIAuNPs on hMSCs

To optimize the concentration of IIAuNPs for hMSC treatment, the viability of hMSCs was evaluated. CCK-8 assay results showed that IIAuNPs did not affect the viability of hMSCs up to 15 μg/mL IIAuNPs. In hMSCs treated with 25 and 50 μg/mL IIAuNPs, 21% and 45% of the cells died, respectively (Fig. 3A). FDA/EB staining images showed that IIAuNPs induced cell death in hMSCs at concentrations higher than 15 μg/mL (Fig. 3B). The TUNEL assay also indicated that apoptotic cells appeared at concentrations higher than 15 μg/mL (Fig. 3C). Taken together, IIAuNPs did not affect the viability of hMSCs up to 15 μg/mL IIAuNPs.

3.3 Phenotype changes in hMSCs after IIAuNP treatment

To assess whether IIAuNP treatment affects the phenotype of hMSCs, we evaluated the gene expression levels of cell survival- and migration-related factors in hMSCs. One hour after treatment with IIAuNPs (15 μg/mL in serum-

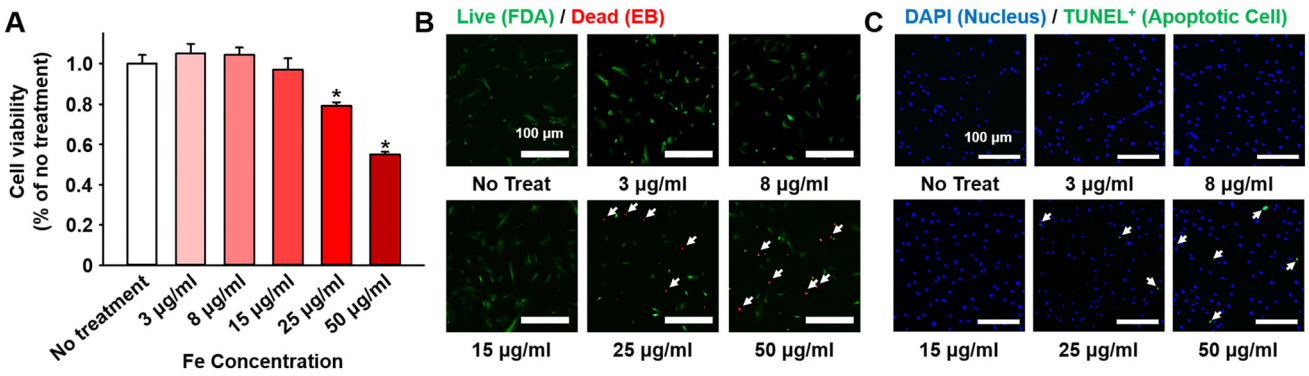

Fig. 3 Cytotoxicity to hMSCs according to the concentration of IIAuNPs. **A** CCK-8 assay after 24 h treatment with IIAuNPs at different concentrations (n = 4, $*p < 0.05$ versus all other group). **B** FDA/EB results showing live cells (green) and dead cells (red) after treating with IIAuNPs at different concentrations. **C** TUNEL assay results showing apoptotic cells (green) and nuclei (DAPI, blue) after treatment with different concentrations of IIAuNPs. White arrows indicate the FDA/EB or TUNEL-positive cells. Scale bars indicate 100 μm

free medium), the gene expression levels of VEGF, FGF2, and CXCR4 were measured by qRT-PCR. The gene expression levels of VEGF, FGF2, and CXCR4 in the IIAuNP treatment group were increased by 1.44, 1.57, and 1.77 times compared to that in the no treatment group (Fig. 4). Since cell viability can be increased with anti-apoptotic factors such as VEGF and FGF2, hMSCs with IIAuNPs injected into a mouse tumor-bearing model might have survived for a long time [15–18]. After culturing the hMSCs with IIAuNPs in a hypoxic environment for 48 h, Bcl-XL and Caspase-3 gene expression was increased by 1.39 and 0.78 times compared to that in the no treatment group (Fig. 4C, D). FDA/EB staining results and quantitative data also showed that IIAuNPs decreased the apoptosis of hMSCs under hypoxic cell culture conditions (Fig. 4E). Additionally, the gene expression level of CXCR4 in IIAuNP-treated hMSCs was increased compared to that in the no treatment group up to 12 h (Fig. 4G, H). To assess the migration ability of IIAuNP-treated hMSCs, we used a scratch assay (Fig. 4J). Treatment of hMSCs with IIAuNPs increased the migration ability of hMSCs. After 18 h of IIAuNP treatment, 6.45% and 8.9% of the empty space between cells were covered in the untreated and IIAuNP-treated groups, respectively (Fig. 4I).

3.4 Photothermal effect *in vitro* and the amount of IIAuNPs in hMSCs

The photothermal effect of IIAuNPs in hMSCs was confirmed by 660 nm laser irradiation. With laser irradiation, the temperature of hMSCs in the no treatment group did not change, whereas that of IIAuNP-treated hMSCs increased over time. Five minutes after the laser irradiation, the temperature of IIAuNP-treated hMSCs increased up to 45.1 °C (Fig. 5A). After treatment with 15 μg/mL IIAuNPs, the amounts Fe and Au in hMSCs were evaluated by ICP-OES (Fig. 5B). In the no treatment group, the amounts of both Au and Fe were not detected.

3.5 PTT and therapeutic effect *in vivo*

After tumor inoculation, PBS, hMSCs, IIAuNPs, and IIAuNPs-hMSCs were injected intravenously. Three days after the injection, the tumor sites were irradiated with a 660 nm laser. Five minutes after the laser irradiation of each group, the temperature of the tumor site increased to 44.85 °C (PBS), 46.3 °C (hMSCs), 49 °C (IIAuNPs), and 53.65 °C (IIAuNPs-hMSCs) (Fig. 6A, B). The ICP-OES results showed that the larger amount of Au was accumulated in tumor tissues compared to the other groups (Fig. 6C). After laser irradiation, the tumor sites were observed for 7 days. In the PBS, hMSC, and IIAuNP-injected groups, the sizes of the tumors did not change after laser irradiation. However, in the IIAuNP-treated hMSCs-injected group, owing to the significant temperature increment, the size of the tumor was dramatically decreased compared to that in other groups (Fig. 6D, E). This result indicates that IIAuNP improved cell migration of hMSCs toward tumors through Fe ion release, and thus, the remaining Au was delivered successfully to the tumor.

4 Discussion

Delivering therapeutic materials using hMSCs has been actively explored for destroying tumors, since hMSCs have the natural property of targeting tumors with high efficiency. In this study, we demonstrated the feasibility of a new PTT method using hMSCs incorporated with Fe ion-releasing nanoparticles. Methods for increasing the efficiency of PTT using hMSCs have been continuously

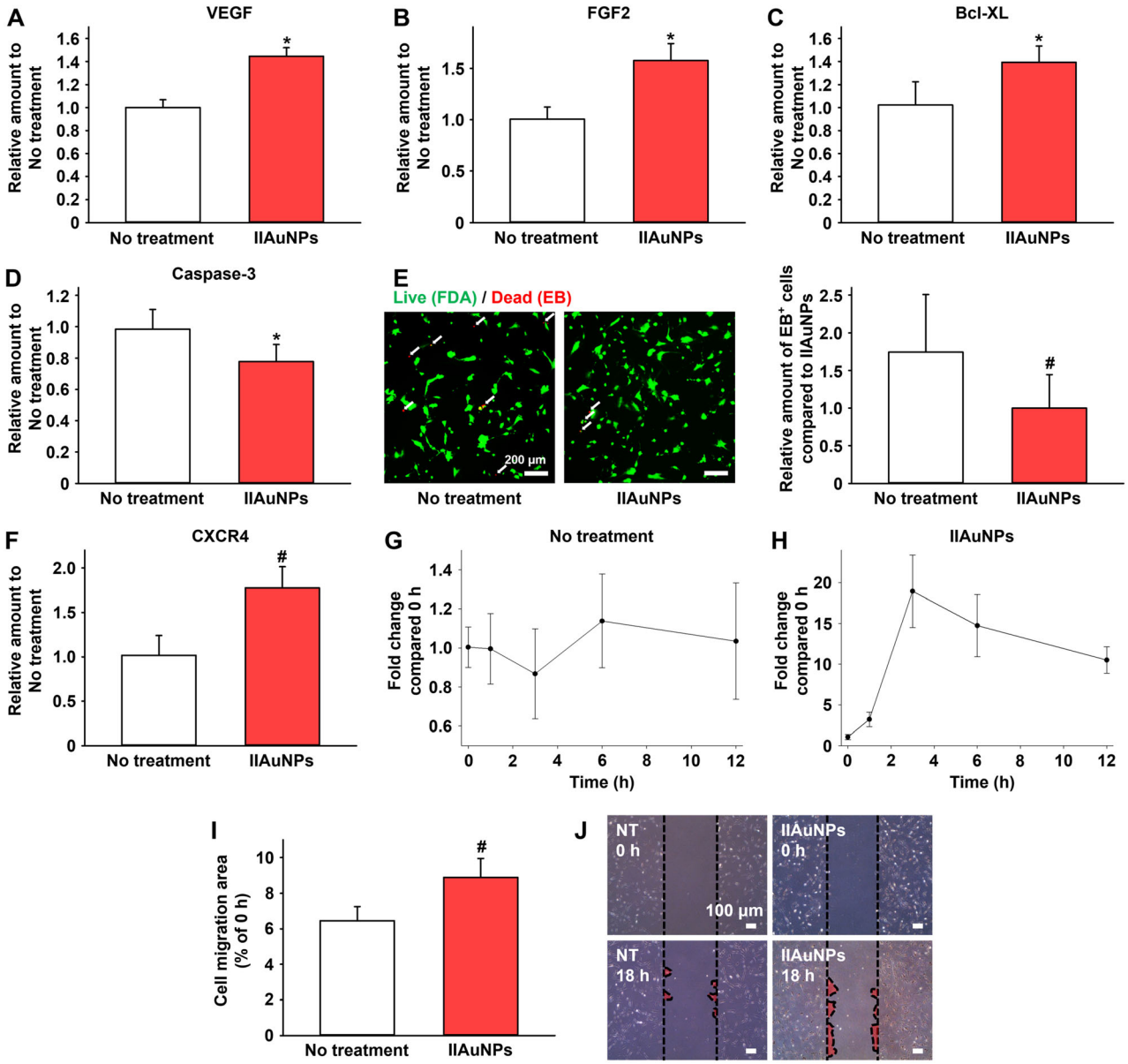

Fig. 4 Enhanced anti-apoptotic paracrine factor expression in hMSCs treated with IIAuNPs. Anti-apoptotic paracrine factor **A** VEGF and **B** FGF2 expression. Anti-apoptotic and apoptotic factor **C** Bcl-XL and **D** Caspase-3 expression after hypoxia conditions for 48 h. **E** FDA/EB results showing live cells (green) and dead cells (red) with quantitative analysis after hypoxia conditions for 48 h (n = 12). Cell migration-related gene, **F** CXCR4 expression in IIAuNP-treated hMSCs was significantly increased compared to that in hMSCs without IIAuNP treatment, as evaluated by qRT-PCR (n = 4, $*p < 0.001$ versus no treatment group, $\#p < 0.05$ versus no treatment group). Maintenance of CXCR4 expression in hMSCs with or without IIAuNPs treatment (**G** NT and **H** IIAuNP-treated hMSCs). **I** Quantification of cell migration area (n = 4, $\#p < 0.05$ versus control group with no treatment) and **J** representative images of migrated hMSCs after 18 h, with or without IIAuNP treatment

reported [5, 23]. The amount of photoreactive nanoparticles in the tumor can be increased through the Trojan horse effect of hMSCs, and thus, the efficiency of PTT can be increased. Since the local temperature increment is proportional to the number of photoreactive nanoparticles, highly accumulate photoreactive nanoparticles in tumor can lead significant temperature increment after the laser irradiation. Temperature increment and following heat generation through laser irradiation can induce critical damage in tumor [6]. Here, we used Fe ions to increase the tumor targeting efficacy of hMSCs. Among the transition metals, Fe was selected and applied to hMSCs to upregulate anti-apoptotic paracrine factor expression for long-term cell circulation after intravenous injection and cell migration ability toward tumors for enhanced targeting efficiency.

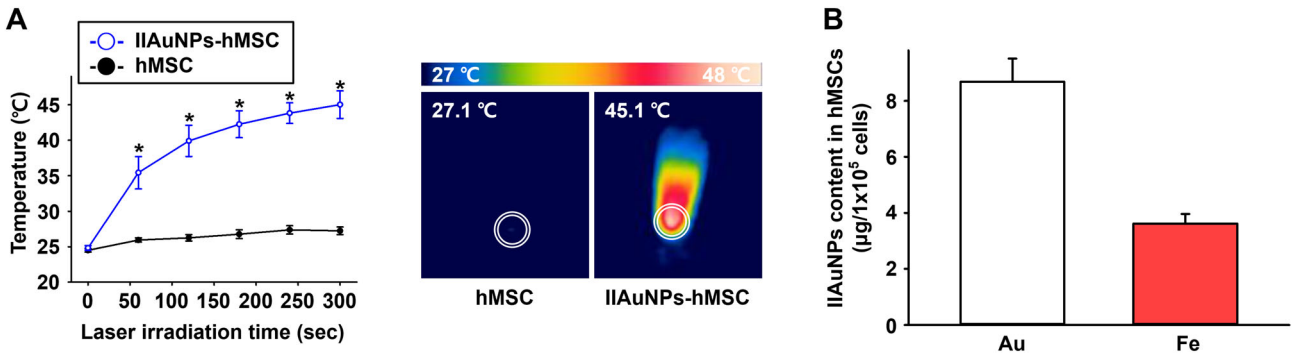

Fig. 5 Amount of IIAuNPs delivered to hMSCs. **A** Results showing the temperature change in hMSCs with or without IIAuNP treatment (n = 4, $*p < 0.001$ versus hMSC group). Representative images showing temperature change 5 min after laser irradiation of hMSCs with or without IIAuNPs. **B** Ratio of Au and Fe in IIAuNPs-hMSC as evaluated by the ICP-OES

Our IIAuNPs were synthesized in an aqueous solution using a co-reduction method, for biomedical applications. IIAuNPs showed good dispersity in water, indicating that they can be easily applied to biomedical applications without further steps such as PEGylation [24]. Small and uniform IIAuNPs readily enter the cell by endocytosis. We showed that Fe ions from IIAuNPs could dissolve at low pH (pH 4.5) in the cell, similar to endosomal conditions (Fig. 2F) [25, 26]. Additionally, the conditions for laser irradiation of newly synthesized IIAuNPs were tested to optimize and maximize the photothermal effect. In general, 660- or 808 nm range lasers are applied for PTT [5, 27, 28]. To confirm the optimum wavelength for IIAuNPs, both 660 nm and 808 nm lasers were used (Fig. 2G, H). The photothermal effect based on heat generation was better when the 660 nm laser was applied to the IIAuNPs compared to the effect of the 808 nm laser treatment. Based on the amount of Au, which is 2.59 times larger than that of Fe in a IIAuNP, we concluded that the 660 nm laser showed a higher photothermal effect than the 808 nm laser, in accordance with other Au-based nanoparticles for PTT.

IIAuNPs with optimized concentration showed no cytotoxicity to hMSCs and sufficient photothermal effect due to enhanced cell viability and tumor-targeted migration. It was necessary to determine the concentration of IIAuNPs that are not toxic to hMSCs. A previous study has shown that the cytotoxicity of Fe is relatively higher than that of Au [29]. Thus, the cytotoxicity of Fe was applied as criteria for optimizing the concentration of IIAuNPs. The final concentration of IIAuNPs for treating hMSCs was 15 μg/mL (Fig. 3A-C). In this study, we focused on the expression of two types of genes that can affect the tumor-targeting efficiency of IIAuNP-loaded hMSCs. One is the gene related to anti-apoptosis, including VEGF and FGF2. Both VEGF and FGF2 are known to enhance cell viability owing to their anti-apoptotic effects [15–18]. In our hMSC-based PTT system, it is important to maintain cell viability for a long period after injection to allow sufficient time to interact with the tumor. Upregulated VEGF and FGF2 secretion from IIAuNP-loaded hMSCs could increase cell viability under *in vivo* conditions, thus leading to high tumor-targeting efficiency. As shown in Fig. 4, VEGF and FGF2 expression in IIAuNP-loaded hMSCs was increased by 1.44 and 1.57 times, respectively, compared to that in hMSCs without IIAuNP treatment. Thus, the cell survival rate was increased in hMSCs treated with IIAuNPs under hypoxic conditions, which mimics the *in vivo* microenvironment. Anti-apoptotic gene expression (Bcl-XL) was enhanced, and pro-apoptotic gene expression (Caspase-3) was decreased in IIAuNP-loaded hMSCs compared to that in the no treatment group. Quantitative data from FDA/EB staining also showed the 1.74 times increased EB^+ cells in hMSCs without any treatment compared to that of hMSCs with IIAuNPs treatment (Fig. 4E). The other type of gene is CXCR4, which is associated with the migration ability of cells. Although the detailed molecular mechanism is not fully understood, previous studies have reported that upregulation of CXCR4 expression could improve tumor-targeting efficiency. Several studies have demonstrated that the interaction between stromal-derived factor 1α and CXCR4 receptors secreted from tumors and CXCR4 in hMSCs is related to tumor-targeted cell migration [14, 30, 31]. The expression of CXCR4 increased by 1.77 times with IIAuNP treatment in hMSCs compared to that in hMSCs without any treatment (Fig. 4F). We also confirmed that CXCR4 expression was increased after IIAuNP treatment and remained high until 12 h (Fig. 4G, H). Upregulation of CXCR4 expression through IIAuNP treatment may have elevated the tumor-targeting capacity of hMSCs.

Through IIAuNP treatment, the *in vivo* therapeutic effect of PTT was significantly improved. When the tumor site was irradiated with the laser in mice injected with IIAuNPs-hMSCs, the temperature increment was the highest compared to that in the other experimental groups

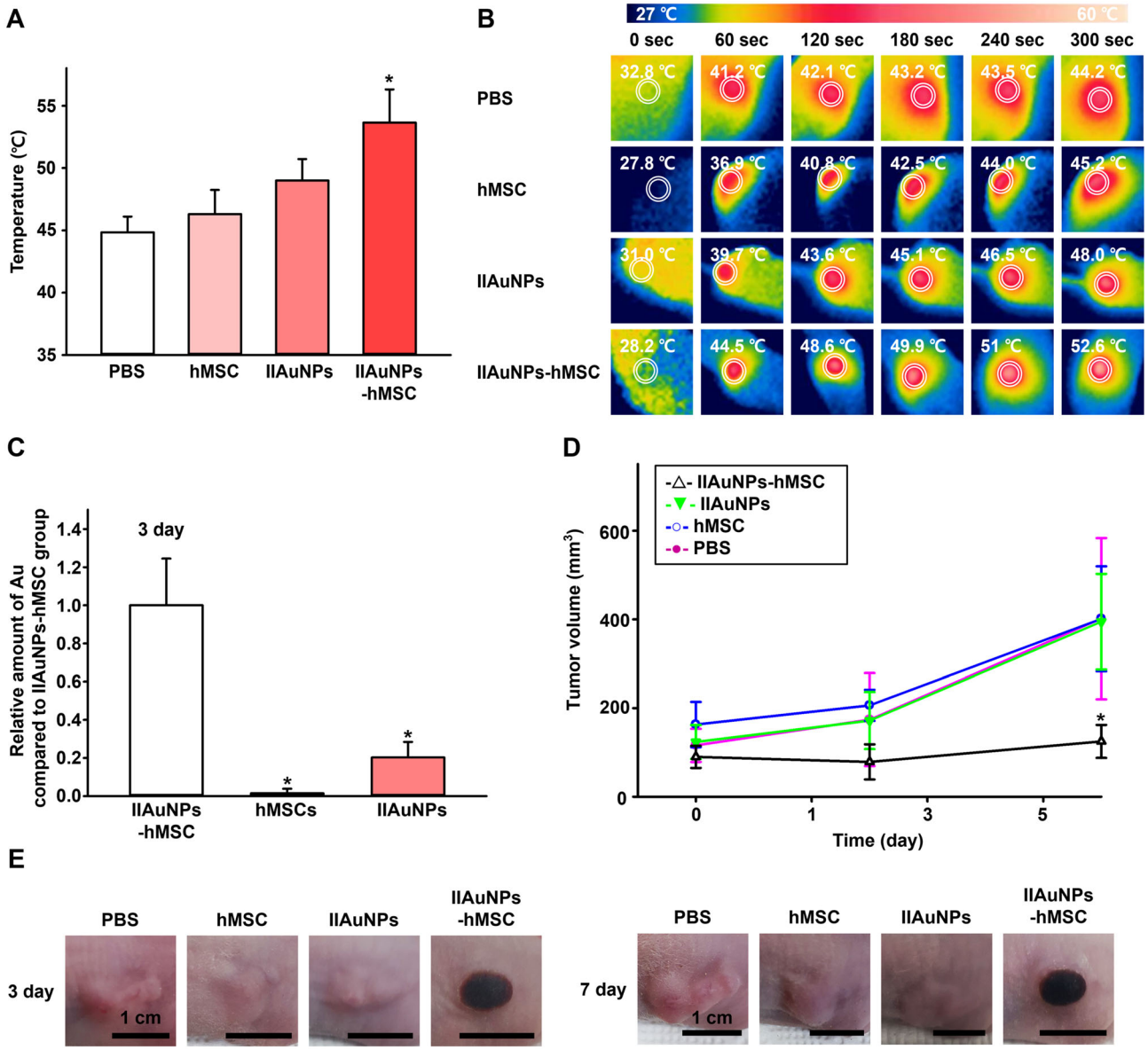

Fig. 6 Temperature changes in tumor after delivering IIAuNPs-hMSCs and therapeutic effect of PTT using IIAuNPs-hMSCs. **A** Temperature change and **B** real-time infrared thermal image in tumor 5 min after laser irradiation in each group (n = 4, $*p < 0.05$ versus all other groups). **C** Relative amount of Au in the tumor 3 days after injecting hMSCs, IIAuNPs, and hMSCs with IIAuNPs (n = 4, $*p < 0.05$ versus IIAuNPs-hMSC groups). **D** Volume change at 7 days after laser irradiation (n = 4, $*p < 0.05$ versus all other groups). **E** Representative images of tumor in each group, 3 and 7 days after the PTT treatment

(Fig. 5A). Since the Fe originally included in IIAuNPs was released in hMSCs as Fe ions after endocytosis, the tumor-targeted cell migration efficacy of hMSCs was upregulated along with enhanced cell survival. Additionally, the amount of gold found in the tumor was also significantly increased in the IIAuNPs-hMSC group compared to other groups. The results indicated that hMSCs preserved their cell viability after intravenous injection through increased intracellular Fe ion concentration and subsequent expression of anti-apoptotic factors. Due to enhanced cell viability, IIAuNP-treated hMSCs could have circulated longer than hMSCs without IIAuNP treatment. Therefore, more gold remaining inside the IIAuNP-treated hMSCs could have reached the tumor site compared to that with the IIAuNP injection. In the *in vivo* experiment, the temperature increment after the laser irradiation was significantly increased in the IIAuNPs-hMSC group compared to that in the PBS, hMSC, and IIAuNP-hMSC groups. Previously, 48 °C was proposed as a standard temperature to induce irreversible damage to tumors using PTT [4]. In our experiment, only the IIAuNPs-hMSC group showed a temperature increase of more than 48 °C. Histological

results and tumor volume quantification data also demonstrated that tumors in the IIAuNPs-hMSC group were severely destroyed compared to those in the other groups (Fig. 6).

In this study, we synthesized IIAuNPs for advanced PTT to treat tumors. IIAuNPs were introduced into hMSCs to improve anti-paracrine factor expression, cell migration ability, and the therapeutic effect of PTT. The synthesized IIAuNPs underwent Fe ionization under mild acid conditions, such as the pH of endosomes. Through our IIAuNPs, the Fe ions were successfully delivered to hMSCs without cytotoxicity and improved the tumor-destroying effect of PTT. The results obtained in our study might support the development of PTT methodology in future based on stem cell and Fe ion delivery systems.

Acknowledgements This research was supported by the National Research Foundation of Korea (NRF), and the Ministry of Science and ICT (NRF-2018M3A9E2023255, NRF-2019R1C1C1007384, NRF-2020M2D9A3094171, NRF-2021R1A4A1032782). This research was also supported by the Korea Medical Device Development Fund grant funded by the Korean government (the Ministry of Science and ICT, Ministry of Trade, Industry and Energy, the Ministry of Health & Welfare, and the Ministry of Food and Drug Safety, Republic of Korea), Project Number: 202011B31.

Compliance with ethical standards

Conflict of interest The authors declare no conflicts of interest relevant to this article.

Ethical Statement All animal treatments and experimental procedures were approved by the Institutional Animal Care and Use Committee of Sungkyunkwan University (No. SKKUIACUC2017-05-03-3). The study protocol was approved by the Institutional Review Board of Sungkyunkwan University (IRB No. 2019-03-002-001). Informed consent was confirmed by the IRB.

References

1. Li Z, Chen Y, Yang Y, Yu Y, Zhang Y, Zhu D, et al. Recent advances in nanomaterials-based chemo-photothermal combination therapy for improving cancer treatment. Front Bioeng Biotechnol. 2019;7:293.
2. Dickerson EB, Dreaden EC, Huang X, El-Sayed IH, Chu H, Pushpanketh S, et al. Gold nanorod assisted near-infrared plasmonic photothermal therapy (PPTT) of squamous cell carcinoma in mice. Cancer Lett. 2008;269:57–66.
3. Gao G, Jiang YW, Sun W, Guo Y, Jia HR, Yu XW, et al. Molecular targeting-mediated mild-temperature photothermal therapy with a smart albumin-based nanodrug. Small. 2019;15:e1900501.
4. Jaque D, Martínez Maestro L, del Rosal B, Haro-Gonzalez P, Benayas A, Plaza JL, et al. Nanoparticles for photothermal therapies. Nanoscale. 2014;6:9494–530.
5. Kang S, Bhang SH, Hwang S, Yoon JK, Song J, Jang HK, et al. Mesenchymal stem cells aggregate and deliver gold nanoparticles to tumors for photothermal therapy. ACS Nano. 2015;9:9678–90.
6. Vines JB, Yoon JH, Ryu NE, Lim DJ, Park H. Gold nanoparticles for photothermal cancer therapy. Front Chem. 2019;7:167.
7. Choi J, Kim SY. Photothermally enhanced photodynamic therapy based on glutathione-responsive pheophorbide a-conjugated gold nanorod formulations for cancer theranostic applications. J Ind Eng Chem. 2020;85:66–74.
8. Willets KA, Van Duyne RP. Localized surface plasmon resonance spectroscopy and sensing. Annu Rev Phys Chem. 2007;58:267–97.
9. Padalar MV, Pleshko N. Wavelength-dependent penetration depth of near infrared radiation into cartilage. Analyst. 2015;140:2093–100.
10. Ullah M, Liu DD, Thakor AS. Mesenchymal stromal cell homing: mechanisms and strategies for improvement. iScience. 2019;15:421–38.
11. Karp JM, Leng Teo GS. Mesenchymal stem cell homing: the devil is in the details. Cell Stem Cell. 2009;4:206–16.
12. Hofer HR, Tuan RS. Secreted trophic factors of mesenchymal stem cells support neurovascular and musculoskeletal therapies. Stem Cell Res Ther. 2016;7:131.
13. Liu Z, Li T, Han F, Wang Y, Gan Y, Shi J, et al. A cascade-reaction enabled synergistic cancer starvation/ROS-mediated/chemo-therapy with an enzyme modified Fe-based MOF. Biomater Sci. 2019;7:3683–92.
14. Huang X, Zhang F, Wang Y, Sun X, Choi KY, Liu D, et al. Design considerations of iron-based nanoclusters for noninvasive tracking of mesenchymal stem cell homing. ACS Nano. 2014;8:4403–14.
15. Ji ST, Kim H, Yun J, Chung JS, Kwon S. Promising therapeutic strategies for mesenchymal stem cell-based cardiovascular regeneration: from cell priming to tissue engineering. Stem Cells Int. 2017;2017:3945403.
16. Tang YL, Zhao Q, Qin X, Shen L, Cheng L, Ge J, et al. Paracrine action enhances the effects of autologous mesenchymal stem cell transplantation on vascular regeneration in rat model of myocardial infarction. Ann Thorac Surg. 2005;80:229–36.
17. Chehelcheraghi F, Chien S, Bayat M. Mesenchymal stem cells improve survival in ischemic diabetic random skin flap via increased angiogenesis and VEGF expression. J Cell Biochem. 2019;120:17491–9.
18. Xia Z, Guo X, Yu N, Zeng A, Si L, Long F, et al. The Application of decellularized adipose tissue promotes wound healing. Tissue Eng Regen Med. 2020;17:863–74.
19. Nezic L, Amidzic L, Skrbic R, Gajanin R, Nepovimova E, Valis M, et al. Simvastatin inhibits endotoxin-induced apoptosis in liver and spleen through up-regulation of survivin/NF-κB/p65 expression. Front Pharmacol. 2019;10:54.
20. Hwang OK, Noh YW, Hong JT, Lee J. Hypoxia pretreatment promotes chondrocyte differentiation of human adipose-derived stem cells via vascular endothelial growth factor. Tissue Eng Regen Med. 2020;17:335–50.
21. Liang CC, Park AY, Guan JL. In vitro scratch assay: a convenient and inexpensive method for analysis of cell migration in vitro. Nat Protoc. 2007;2:329–33.
22. Gebäck T, Schulz MM, Koumoutsakos P, Detmar M. TScratch: a novel and simple software tool for automated analysis of monolayer wound healing assays. Biotechniques. 2009;46:265–74.
23. Park JH, Yoon JK, Kim YJ, Lee TJ, Jeong GJ, Kim DI, et al. Enhancing therapeutic efficacy of photothermal therapy using poloxamer-reduced graphene oxide and mesenchymal stem cells. J Ind Eng Chem. 2019;80:846–53.
24. Chen CC, Chang DY, Li JJ, Chan HW, Chen JT, Chang CH, et al. Investigation of biodistribution and tissue penetration of PEGylated gold nanostars and their application for photothermal cancer treatment in tumor-bearing mice. J Mater Chem B. 2020;8:65–77.
25. Im GB, Jung E, Kim YH, Kim YJ, Kim SW, Jeong GJ, et al. Endosome-triggered ion-releasing nanoparticles as therapeutics

to enhance the angiogenic efficacy of human mesenchymal stem cells. J Control Release. 2020;324:586–97.
26. Kim YH, Jung E, Im GB, Kim YJ, Kim SW, Jeong GJ, et al. Regulation of intracellular transition metal ion level with a pH-sensitive inorganic nanocluster to improve therapeutic angiogenesis by enriching conditioned medium retrieved from human adipose derived stem cells. Nano Converg. 2020;7:34.
27. Bucharskaya A, Maslyakova G, Terentyuk G, Yakunin A, Avetisyan Y, Bibikova O, et al. Towards effective photothermal/photodynamic treatment using plasmonic gold nanoparticles. Int J Mol Sci. 2016;17:1295.
28. Park S, Lee WJ, Park S, Choi D, Kim S, Park N. Reversibly pH-responsive gold nanoparticles and their applications for photothermal cancer therapy. Sci Rep. 2019;9:20180.
29. Sabella S, Carney RP, Brunetti V, Malvindi MA, Al-Juffali N, Vecchio G, et al. A general mechanism for intracellular toxicity of metal-containing nanoparticles. Nanoscale. 2014;6:7052–61.
30. Kalimuthu S, Zhu L, Oh JM, Gangadaran P, Lee HW, Baek SH, et al. Migration of mesenchymal stem cells to tumor xenograft models and in vitro drug delivery by doxorubicin. Int J Med Sci. 2018;15:1051–61.
31. Van Nguyen TT, Vu NB, Van Pham P. Mesenchymal stem cell transplantation for ischemic diseases: mechanisms and challenges. Tissue Eng Regen Med. 2021;18:587–611.